Applied Catalysis B: Environmental 203 (2017) 820–828

Contents lists available at ScienceDirect

Applied Catalysis B: Environmental

journal homepage: www.elsevier.com/locate/apcatb

Novel nanoporous N-doped carbon-supported ultrasmall Pd nanoparticles: Efficient catalysts for hydrogen storage and release

Katherine Koh[a,1], Mina Jeon[b,1], Daniel M. Chevrier[c], Peng Zhang[c], Chang Won Yoon[b,d,**], Tewodros Asefa[a,e,*]

[a] Department of Chemistry and Chemical Biology, Rutgers, The State University of New Jersey, Piscataway, NJ 08854, USA
[b] Fuel Cell Research Center, Korea Institute of Science and Technology, Seoul 136-791, Republic of Korea
[c] Department of Chemistry, Dalhousie University, Halifax, Nova Scotia B3H 4R2, Canada
[d] KHU-KIST Department of Converging Science and Technology, Kyung Hee University, Seoul, Republic of Korea
[e] Department of Chemical and Biochemical Engineering, Rutgers, The State University of New Jersey, Piscataway, NJ 08854, USA

ARTICLE INFO

Article history:
Received 19 July 2016
Received in revised form 19 October 2016
Accepted 28 October 2016
Available online 29 October 2016

Keywords:
Hydrogen storage
Hydrogen release
Pd/Carbon nanomaterial
Formate dehydrogenation
Bicarbonate hydrogenation

ABSTRACT

The reversible reactions involving formate and bicarbonate can be used to store and release hydrogen (H_2), allowing H_2 to serve as an effective energy carrier in energy systems such as fuel cells. However, to feasibly utilize these reactions for renewable energy applications, efficient catalysts that can reversibly promote both reactions are required. Herein we report the synthesis of novel polyaniline (PANI)-derived mesoporous carbon-supported Pd nanoparticles, or materials that can efficiently catalyze these reversible reactions. The synthesis involves pyrolysis of PANI/colloidal silica composite materials at temperatures above 500 °C, followed by removal of the colloidal silica from the carbonized products with an alkaline solution and finally deposition of Pd nanoparticles within the mesoporous carbon products. The resulting nanomaterials efficiently catalyze the reversible reactions, *i.e.*, the dehydrogenation of formate ($HCO_2^- + H_2O \rightarrow H_2 + HCO_3^-$) and the hydrogenation of bicarbonate ($H_2 + HCO_3^- \rightarrow H_2O + HCO_2^-$). The porosity and the catalytic property of the materials can be tailored, or improved, by changing the synthetic conditions (in particular, the pyrolysis temperature and the amount of colloidal silica used for making the materials). The study further reveals that having an optimum density of N dopant species in the catalysts makes Pd to exhibit high catalytic activity toward both reactions. Among the different materials studied here, the one synthesized at 800 °C with relatively high amount of colloidal silica template gives the best catalytic activity, with a turnover frequency (TOF) of 2,562 h^{-1} for the dehydrogenation reaction and a turnover number (TON) of 1,625 for the hydrogenation reaction.

1. Introduction

In the face of the rising energy consumptions worldwide and the continued negative environmental impacts caused by fossil fuels, there are burgeoning efforts to find alternative energy sources and carriers [1–3]. These efforts include research in hydrogen (H_2), which has long been regarded as one of the most promising energy carriers, because it is a clean and renewable fuel [4,5]. While hydrogen's use in fuel cells has long been successfully demonstrated, finding efficient hydrogen storage systems that can make hydrogen-based energy technologies sustainable and widely applicable still remains a challenge [6,7]. To address these issues, several chemical systems that inherently possess high hydrogen density and that can release H_2 hydrolytically or thermally, such as sodium borohydride or ammonia borane, have been widely studied [8,9]. However, the reaction pathways that these systems follow while releasing H_2 make them difficult to deploy, because their spent fuels are in solid phase or in slurry form, and are thus hard to regenerate back to fuels [10,11]. This is, in fact, one of the major stumbling blocks limiting the utilization of these systems as efficient, safe, and reversible hydrogen storage/release media.

Owing to their regenerability and high volumetric hydrogen content, formic acid (HCO_2H) and related compounds are more interesting reversible hydrogen storage/release systems [12,13]. Recently, the Beller [14,15] and the Joó [16] groups showed that the formate/bicarbonate (HCO_2^-/HCO_3^-) reversible reactions over

* Corresponding author at: Department of Chemistry and Chemical Biology, Rutgers, The State University of New Jersey, Piscataway, NJ, 08854, USA.
** Corresponding author at: Fuel Cell Research Center, Korea Institute of Science and Technology, Seoul, 136-791, Republic of Korea.
E-mail addresses: cwyoon@kist.re.kr (C.W. Yoon), tasefa@rci.rutgers.edu (T. Asefa).
[1] K. Koh and M. Jeon contributed equally to this work.

http://dx.doi.org/10.1016/j.apcatb.2016.10.080
0926-3373/

homogeneous Ru-based catalysts enable a rechargeable hydrogen battery. In fact, compared with the HCO_2H/CO_2 system, a system that has been more widely studied for H_2 storage/release, the HCO_2^-/HCO_3^- system can be more advantageous, especially for fuel cell applications. This is because the latter: 1) tends to release H_2 without producing CO, a known poison for the Pt and other catalysts commonly used in fuel cells, and 2) can release the H_2 under non-acidic media, the media that is sometimes preferred for reactions employed in various fuel cells. However, so far only few *heterogeneous* catalysts have been studied for catalytic inter-conversions of HCO_2^-/HCO_3^-, and they include Pd/C [17,18] and reduced graphene oxide-supported Pd nanoparticles (Pd/r-GO) [19]. More importantly, some of these previous studies have revealed that, when supported on carbon materials, Pd could give comparable catalytic activity as, and better selectivity and reversibility than, its homogenous counterparts for the HCO_2^-/HCO_3^- reversible reactions [17–21].

Meanwhile, it has been reported that by doping the structure of carbon support materials with heteroatoms (*e.g.*, N [22–24], B [25], or P [26]), not only the physical and chemical properties of the materials can be favorably tailored, but also the ability of the materials to assist supported catalytically active metallic species on them (*e.g.*, Pd nanoparticles or Ru complexes) to catalyze reactions can be improved [22–27]. Moreover, although the exact mechanisms are not yet well understood, N-based species in amine-functionalized mesoporous silicas or carbon nitrides have been known to provide some synergetic effects with various metallic catalytic groups, especially Pd nanoparticles, and make the latter to cooperatively promote the deprotonation step involved in formic acid dehydrogenation [22–26]. Besides, many N-based moieties are known for their ability to stabilize Pd nanoparticles, increasing the latters' shelf-lives during catalysis. However, despite their similar, favorable surface properties as amine groups (such as polarity and basicity), the potential of the N-dopants of N-doped carbon materials to assist with the HCO_2^-/HCO_3^- reversible reactions has been rarely explored [17–21]. In other words, the ease of tailorability of the properties of carbon support materials *via* heteroatom doping [27], and the possible advantages this may have on the catalytic activity of the resulting heterogeneous catalysts toward HCO_2^-/HCO_3^- reversible reactions, have not been investigated.

To this end, herein we report the synthesis of novel polyaniline (PANI)-derived mesoporous N-rich carbon materials with Pd nanoparticles (Pd/PDMCs) (Scheme 1) that show efficient catalytic activity toward HCO_2^-/HCO_3^- reversible reactions. To synthesize the catalysts, PANI is used as a precursor and silica nanoparticles are used as templates. PANI is purposely chosen as a precursor because it has a high N/C atomic ratio (0.167), and can thus give a relatively high yield of N-dopant species in the carbon materials upon pyrolysis [28]. Silica nanoparticles are used as templates in order to render the carbon support materials high porosity and large surface area so that the catalysts can have better diffusion pathways for the reactants and products, and give better catalytic activity [29]. Additionally, by applying different pyrolysis temperatures, the density and the type of N-doped species in the PANI-derived mesoporous carbon materials are tailored, and the materials' catalytic properties are further are optimized/improved.

2. Experimental section

2.1. Synthesis of polyaniline-derived mesoporous carbons (PDMCs)

First, a nanocomposite material composed of polyaniline (PANI)/silica nanoparticles was synthesized with oxidative polymerization [30] of aniline in the presence of silica nanoparticles. Typically, an aqueous solution (100 mL) containing 1.0 M formic acid was stirred with 20 mmol of $(NH_4)_2S_2O_8$ at 2 °C until all the reagents were completely dissolved. Then, various amounts (0, 4, 8 or 16 g) of Ludox® HS-40 colloidal silica (40 wt.% in H_2O) were added drop-wise into the solution under vigorous stirring. While the mixture was still stirring, 20 mmol of aniline was slowly added. The mixture was further stirred at 2 °C for 24 h and the solid product was then separated (*via* centrifugation at 15,000 rpm for 20 min, followed by decantation, and washing with H_2O (3 times) and EtOH (2 times)). The resulting material was dried at 60 °C in vacuum oven for 12 h. Finally, a dark blue-to-greenish colored product, *i.e.*, PANI/silica nanocomposite material, was obtained.

The resulting material was subjected to pyrolysis under Ar atmosphere in a temperature-programmable tube furnace at various temperatures (500, 700, 800, 900, or 1000 °C). The pyrolysis process was programmed to involve: 1) heating the material from room temperature to 300 °C at a heating rate of 1 °C min^{-1} and keeping the temperature at 300 °C for 3 h and 2) increasing the pyrolysis temperature from 300 to 500, 700, 800, 900, or 1000 °C at a heating rate of 10 °C min^{-1} and keeping the temperature there for an additional 2 h.

The resulting black powdered products were treated with 1.0 M NaOH solution in an autoclave at 100 °C for 18 h to remove the silica templates in them. After filtration, the solid products were washed with copious amounts of water and EtOH, and let to dry at 40 °C under vacuum. This finally yielded a series of black powdered materials, labeled as PDMC-*T*-*x* (where *T* represents their pyrolysis temperature and *x* represents the amount of colloidal silica in g per 0.02 mol of aniline used to make the precursors of the PDMCs).

2.2. Synthesis of Pd/PDMC materials

To generate supported Pd nanoparticles in the PDMCs materials, first 200 mg of each one of the PDMC-*T*-*x* materials was placed in an aqueous solution (40 mL) containing 56 μmol $Pd(NO_3)_2{\cdot}2H_2O$. (For the synthesis of PDMC with a lower loading of Pd nanoparticles, 19 μmol of $Pd(NO_3)_2{\cdot}2H_2O$ was used instead). The mixtures were stirred at room temperature for 3 h and then filtered, and the solid products were washed with distilled water. The resulting solid products were dried at 40 °C under vacuum. Finally, the Pd(II)-loaded PDMC-*T*-*x* materials were subjected to thermal treatment at 250 °C in N_2/H_2 (90/10%) atmosphere for 3 h to reduce the Pd(II) ions to Pd(0) atoms. This finally led to brown-colored, Pd nanoparticles-containing PDMC-*T*-*x* powder materials. The materials were denoted as Pd/PDMC-*T*-*x*, where again *T* represents their final pyrolysis temperature and *x* represents the amount of colloidal silica in g used per 0.02 mol of aniline to make the PDMCs.

2.3. Catalytic dehydrogenation of sodium formate

To test the catalytic properties of the materials toward formate dehydrogenation, typically 25 mg of one of Pd/PDMC-*T*-*x* materials was added into an aqueous solution of 5 mL, 1.0 M sodium formate (HCO_2Na). The reaction mixture was stirred, and the amount of H_2 evolved from the reaction was determined as follows. The gaseous product produced by the reaction was let to pass through a NaOH (10 M) trap to remove the CO_2 byproduct as well as any possible water vapor forming from the reaction. The remaining gaseous product was then measured using a gas burette in real time at room temperature. Additionally, a blank experiment with the same experimental set up, containing 5 mL of 1 M of sodium formate, but without a catalyst was performed.

To analyze the composition of the gaseous product evolved, one of the outlets of the reactor was connected to a gas sampling bag, and the product collected there from the reaction was analyzed with gas chromatography (GC). For kinetic isotope effect (KIE) stud-

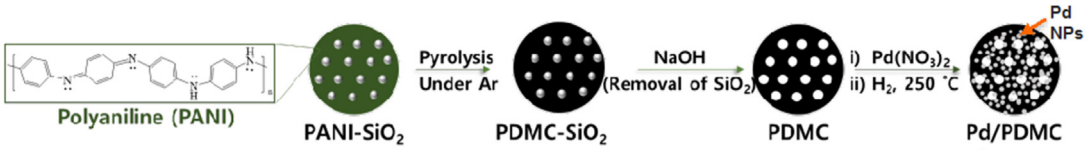

Scheme 1. Schematic illustration of the synthesis of PANI-derived mesoporous N-doped carbon-supported Pd nanoparticles (Pd/PDMC) materials.

ies, two deuterated reagents (DCO_2Na and D_2O) were used instead of HCO_2Na and H_2O under otherwise similar experimental procedures.

2.4. Catalytic hydrogenation of sodium bicarbonate

Typically, a mixture of 50 mg of one of the Pd/PDMC-*T*-*x* catalysts and 10 mL of 1.0 M aqueous solution of sodium bicarbonate (HCO_3Na) were mixed in a stainless steel reactor and then purged with N_2. H_2 gas was then let to flow into the reactor till the pressure in the reactor reached 40 bar. The reaction mixture was heated to a desired temperature (*i.e.*, 80 °C in our case) and stirred for 24 h while continuously H_2 gas was continuously flowing in it and while the reactor's pressure was maintained constant (40 bar). After letting it to cool down to room temperature, the reactor was depressurized, and the reaction mixture was purged with N_2 before it was finally exposed to air. The catalyst was removed from the reaction mixture by a syringe filter, and the liquid collected was analyzed using high-performance liquid chromatography (HPLC).

2.5. Recyclability tests of the catalysts

The recyclability of the catalysts was evaluated by recovering them from the reaction mixtures. Typically, after the reaction, the spent catalyst was recovered by filtration, and washed several times with deionized water and then ethanol (*via* stirring, centrifugation, and decantation). The recovered catalyst was then dispersed in deionized water (100 mL) and stirred overnight to remove the products or reagents adsorbed on its surfaces. The catalyst was dried under vacuum oven after filtration, and then used as catalyst in the next reaction cycle. This procedure was repeated several times as necessary.

3. Results and discussion

3.1. Synthesis and characterization of catalysts

The synthetic procedure used to make Pd/PDMCs consists of three steps. First, *in-situ* polymerization of PANI within the void spaces of different amounts of colloidal silica templates is carried out (Scheme 1). The resulting PANI-silica composite materials are pyrolyzed at 300 °C for 3 h, and then at 500, 700, 800, 900 or 1000 °C for 2 h, under argon atmosphere. Following this, the silica nanoparticles in the carbonized products are etched with an aqueous NaOH solution. The resulting PANI-derived mesoporous carbons, denoted PDMCs, are immobilized with Pd(II) ions, and the Pd(II) ions-immobilized PDMCs are then subjected to reduction at 250 °C in 10% H_2/90% N2 atmosphere to generate Pd(0) nanoparticles in the PDMCs. Finally, Pd/PDMC-*T*-*x* materials, in which *T* represents the final pyrolysis temperature and *x* represents the amount of colloidal silica (in g) per 0.02 mol of aniline used to make the PDMCs, are obtained. The as-synthesized Pd/PDMC materials prepared using different (i) amounts of colloidal silica (see below) and (ii) calcination temperatures (see below) are then characterized and used as catalysts for formate-bicarbonate reversible reactions to provide valuable information about the effect of the synthetic conditions on the structures, compositions, and catalytic properties of the materials.

3.2. Effect of colloidal silica on the structures of PDMC-T-x materials

First, the effect of the added colloidal silica on the textural properties and morphology of the PDMC-*T*-*x* materials are examined by using N_2 gas adsorption/desorption, scanning transmission electron microscopy (STEM), and high-resolution transmission electron microscopy (HR-TEM). In all the cases, the adsorption/desorption isotherms are found to be Type IV with hysteresis loops, indicating the presence of mesoporous structure in them (entries 1–4 in Table 1 and Fig. S1). However, larger surface areas are found in the materials synthesized using colloidal silica templates, and a relatively much lower surface area is obtained in the material synthesized without using colloidal silica template. These results are further confirmed by HR-TEM images, which show the presence of porosity in all of the Pd/PDMC materials (Fig. 1a, b and S2). But, the highest porosity is found in Pd/PDMC-1000-16 (the material synthesized using relatively higher amount of colloidal silica as template) while the lowest porosity is found in Pd/PDMC-1000-0 (the control material synthesized without using colloidal silica as template). So, these results reveal that the structures of the Pd/PDMC materials vary depending on if and how much colloidal silica is used as template for the synthesis of the materials.

Besides aiding with the formation of porous structures, the colloidal silica particles used as templates in the syntheses of the materials appear to have indirectly helped with the formation of small Pd nanoparticles in the final materials. Specifically, when *x* (the amount of colloidal silica) is increased from 0 to ≥ 4 g, the size of the Pd nanoparticles in Pd/PDMC-1000-*x* materials becomes smaller, or their average size decreases from *ca.* 16 nm to *ca.* 1.5–1.7 nm (Fig. 1a, 1b and S2). Additionally, results obtained by inductively coupled plasma optical emission spectrometry (ICP-OES) show that the colloidal silica templates seem to assist with the loading of Pd onto the PDMC materials. In other words, although 282 μmol Pd(II)/$g_{catalyst}$ is employed to synthesize the Pd nanoparticles in all of the Pd/PDMC-1000 materials, the μmol Pd/g_{cat} that end up residing in the final materials after the reduction step varies between 70 μmol/gcat and 230 μmol/gcat. More specifically, the amount of Pd in Pd/PDMC-1000-0 (made without colloidal silica template) is much smaller (70 μmol/g_{cat}) than the amounts (180–230 μmol/g_{cat}) obtained in the materials synthesized using colloidal silica templates (*i.e.*, Pd/PDMC-1000-4, Pd/PDMC-1000-8 and Pd/PDMC-1000-16 (Entry 1-4, Table 1)).

3.3. Effect of pyrolysis temperature on the structures of PDMC-T-x materials

The textural properties of the series of Pd/PDMC-*T*-16 materials synthesized at different pyrolysis temperatures (500, 700, 800, 900, or 1000 °C) are then evaluated (Fig. 1 and entries 4–8 in Table 1). Compared with Pd/PDMC-500-16 (whose BET surface area is 510 $m^2\,g^{-1}$), the materials obtained at 700 °C or higher pyrolysis temperatures all show significantly higher surface areas and porosity (with BET surface areas between 845 and 1080 $m^2\,g^{-1}$).

Table 1
Textural properties of Pd/PDMC-*T*-*x* materials and the average size of their Pd nanoparticles as a function of the amount of colloidal silica templates and pyrolysis temperatures used to synthesize the materials.

Entry	Pd/PDMC-*T*-*x*		A_{BET} [$m^2\ g^{-1}$][a]	D_{BJH}[nm][b]	V[$cm^3\ g^{-1}$][c]	Pd[μmol/g_{cat}][d]	Average size of Pd Nanoparticles [nm][e]
	T	*x*					
1	1,000	0	260	2.5	0.2	70	16.0
2	1,000	4	817	7.4	1.5	230	1.5
3	1,000	8	919	8.0	1.8	200	1.5
4	1,000	16	994	9.7	2.4	180	1.7
5	900	16	934	9.2	2.2	150	1.6
6	800	16	1,080	9.4	2.5	140	1.6
7	700	16	845	8.4	1.8	150	1.5
8	500	16	510	3.4	0.4	130	1.7

[a] BET surface area.
[b] Average pore diameter obtained from the desorption branch of N_2 absorption/desorption data.
[c] Pore volume.
[d] Measured by ICP-OES.
[e] Determined by STEM.

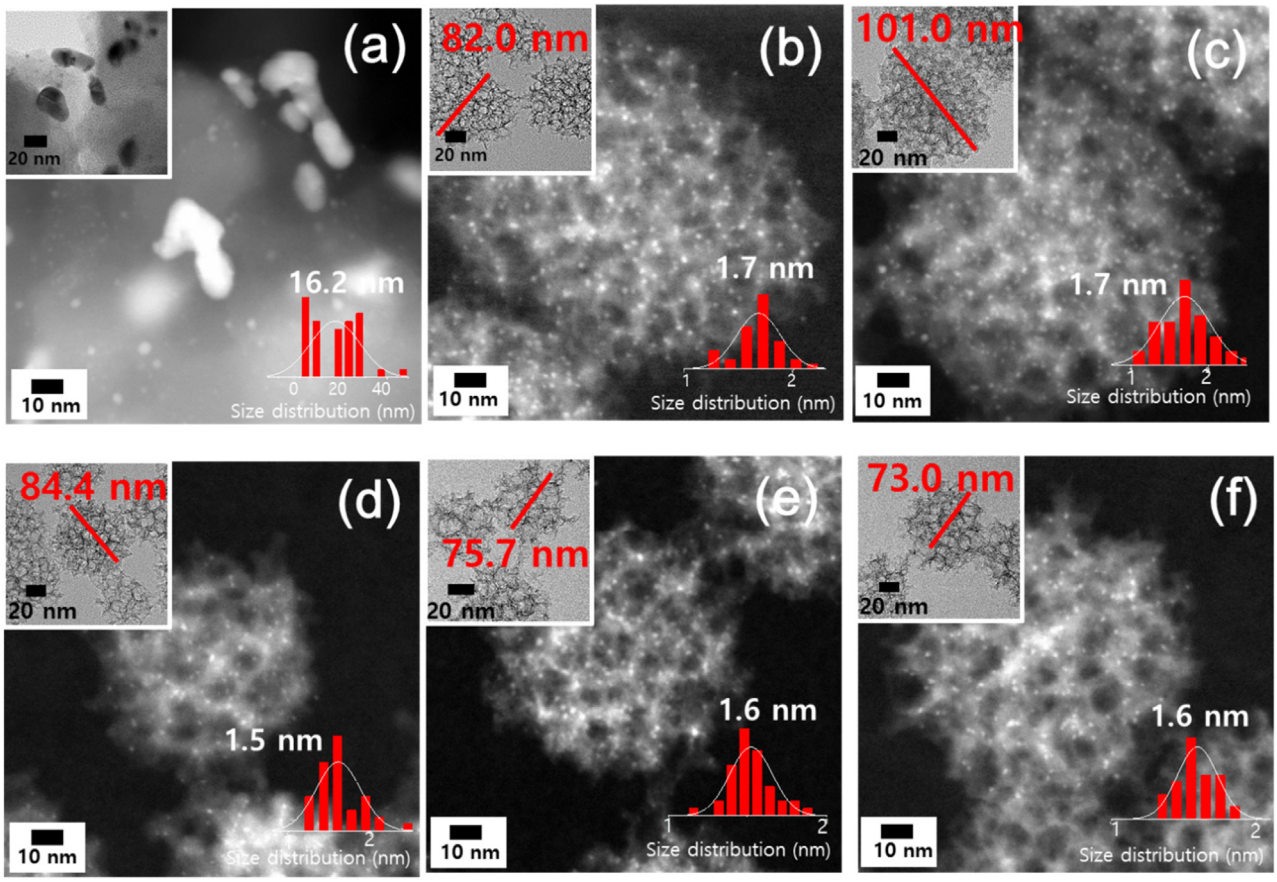

Fig. 1. STEM and TEM images (inset) of Pd/PDMC-*T*-*x* materials: (a) Pd/PDMC-1000-0 (a control material), (b) Pd/PDMC-1000-16, (c) Pd/PDMC-500-16, (d) Pd/PDMC-700-16, (e) Pd/PDMC-800-16, and (f) Pd/PDMC-900-16.

Close examination of the materials' morphologies by STEM and TEM reveal that Pd/PDMC-500-16 has larger, elliptical-shaped mesoporous carbon nanoparticles (*ca.* 101 nm) whereas those obtained at higher pyrolysis temperatures (700 °C and higher) have relatively smaller, spherical mesoporous carbon nanoparticles (with sizes ranging from 73 to 84 nm) (Fig. 1). The size of the Pd nanoparticles in the materials is, however, reasonably similar in all of them (with an average size of *ca.* 1.6 nm), except in the one made without using colloidal silica as templates, in which case their size is much higher, with a value of *ca.* 16 nm. The amount of Pd in the PDMC-*T*-16 materials (*T* = 500, 700, 800, 900 and 1000 °C) determined by ICP-OES is *ca.* 130–180 μmol/g_{cat} (Table 1). Furthermore, by lowering the amount of Pd(II) from 282 to 94 μmol/g_{cat} in PDMC-800-16 support material, Pd(0)/PDMC-800-16 containing 80 μmol/g_{cat} of Pd(0) is obtained. The XRD patterns of the materials show a weak peak at around 2Θ = 40° corresponding to the (111) Bragg reflection of Pd, besides a peak at *ca.* 2Θ = 24 °corresponding to the (002) plane of amorphous/graphitic carbon (Fig. S3).

3.4. *Catalytic properties of Pd/PDMC-T-x for* HCO_2^- *dehydrogenation*

The catalytic properties of the Pd/PDMC-*T*-*x* materials are tested, first for the HCO_2^- dehydrogenation reaction (Table 2). The con-

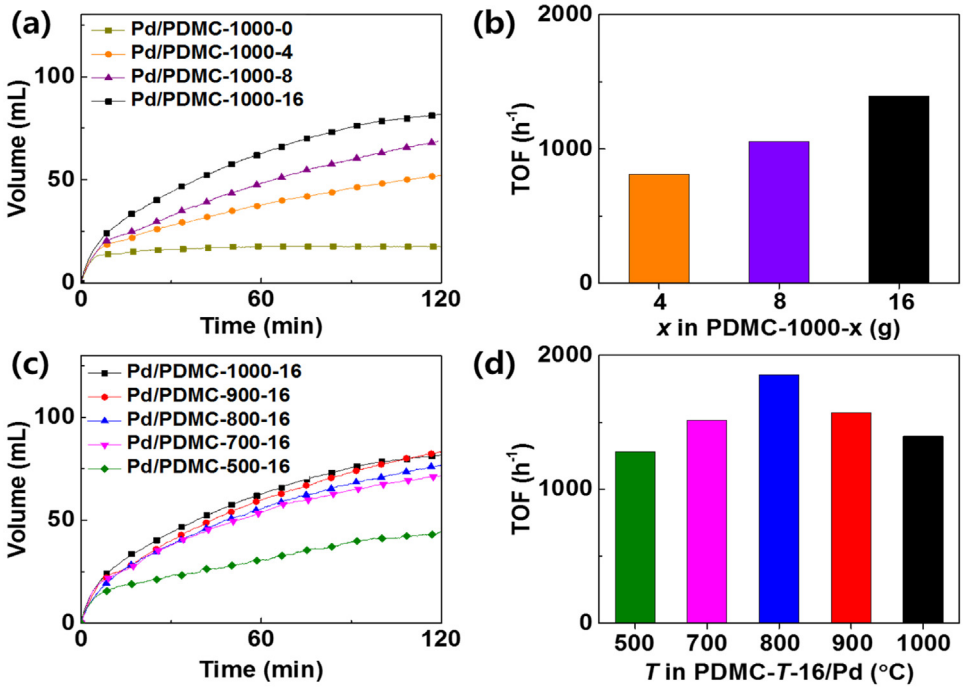

Fig. 2. Amount of catalytically produced H_2 versus reaction time during the dehydrogenation of 1 M of aqueous $NaHCO_2$ over the different Pd/PDMC materials (left panels) and comparison of the relative catalytic activity of the materials in the reaction (right panels) for: (a,b) the series of Pd/PDMC-1000-*x* materials and (c,d) the series of Pd/PDMC-*T*-16 materials.

Table 2
Catalytic TOF values for the dehydrogenation of sodium formate ($NaHCO_2$) over the Pd/PDMC-*T*-*x* materials/catalysts.[a]

Entry	Pd/PDMC-*T*-*x*		TOF[h^{-1}][b]
	T	*X*	
1	1,000	0	N/A
2	1,000	4	813
3	1,000	8	1,054
4	1,000	16	1,396
5	900	16	1,570
6	800	16	1,854
7[c]	800	16	2,562
8	700	16	1,515
9	500	16	1,281
10[d,e]	Pd/C	N/A	1,034

[a] All the reactions are carried out in 5 mL of 1 M of sodium formate with 25 mg of catalyst at 80 °C.
[b] TOF is calculated using the data obtained at 10 min using Eq. (2) in Table S1.
[c] 80 μmol/g_{cat} is loaded on the support material by using 94 μmol/g_{cat} of Pd(II) during the synthesis.
[d] 5 mg (4.7 μmol) of Pd/C, 10 wt.% (commercially available from Sigma-Aldrich) is used.
[e] Note that the surface area of this material is also high (745 m^2/g) or is comparable to those of most of the Pd/PDMC materials.

trol material (Pd/PDMC-1000-0, entry 1 in Table 2) shows barely any catalytic activity toward the reaction (Fig. 2). On the other hand, the materials prepared using colloidal silica templates show good catalytic activity toward the reaction. Furthermore, their catalytic performances for conversion of the reactants and turnover-frequency (TOF) increase when the amount of colloidal silica (*x*) used to make the materials is increased from 4 to 16 g (see entries 2–4 in Table 2 and Fig. 2a,b). Since the size of the Pd nanoparticles is nearly identical in all the Pd/PDMC-*T*-*x* materials, this trend in catalytic activity is most likely to do with the increase in surface area in the Pd/PDMC-1000-*x* (as the result of the increase in the relative amount of colloidal silica used (*x*) to synthesize them).

Additionally, the catalytic activity of the materials toward the reaction (*i.e.*, HCO_2^- dehydrogenation) is found to depend on the pyrolysis temperature used to synthesize them. The relationship follows a volcano type trend, where the catalytic activity of the materials increases as the pyrolysis temperature is raised from 500 to 800 °C, but then decreases afterwards (see entries 4–9 in Table 2 and Fig. 2c–d). Based on this result, it can be said that Pd/PDMC-800-16 is the best catalyst for HCO_2^- dehydrogenation reaction among the series of materials we have investigated here. Actually, when the loading of Pd(0) on PDMC-800-16 is intentionally lowered from 140 to 80 μmol/g_{cat}, by decreasing the relative amount of Pd(II) used to synthesize the Pd nanoparticles from 282 to 94 μmol/g_{cat}, the TOF of the resulting material for HCO_2^- dehydrogenation is significantly higher, with a TOF value of 2,562 h^{-1} (entry 7 in Table 2). Since the size of the Pd nanoparticles in the two materials is found to be about the same and the loading efficiency is effectively similar, there must have been relatively less number of Pd nanoparticles in the pores of the latter material. This, in turn, makes the latter material to provide better pathways for diffusion of reactants and products, and then yield better catalytic yield. This is what, we believe, is responsible for the higher TOF value obtained for the PDMC-800-16 material containing less amount of Pd compared with the one with higher amount of Pd.

Notably also, the catalytic activity of Pd/PDMC-800-16 is higher than those of Pd/C [17,18] and Pd/NMC [20] (or the few heterogeneous catalysts reported for the reaction in the literature) (Table S1). Moreover, Pd/PDMC-800-16's catalytic activity for the dehydrogenation reaction is better than that of the commercially available Pd/C material containing no N dopants in its carbon structure as well (entry 10 in Table 2). So, based on these comparative results, it appears that the N sites incorporated into the PDMC support material are instrumental to the enhanced catalytic activity exhibited by the Pd/PDMC-800-16 as well as the other Pd/PDMC materials. This point is discussed further in the sections to follow.

It is worth adding that the dehydrogenation reaction over the Pd/PDMC-*T*-*x* materials does not release CO, as characterized by

Table 3
Turnover number (TON) values for the hydrogenation of sodium bicarbonate (HCO_3^-) over Pd/PDMC-*T*-16.[a]

Entry	PDMC-*T*-*x*		Conv. [%][b]	TON[c]
	T	x		
1	500	16	22	338
2	700	16	74	987
3	800	16	82	1,171
4[d]	800	16	65	1,625
5	900	16	73	973
6	1,000	16	70	778
7[e,f]	Pd/C	N/A	52	369

[a] Reaction conditions: 50 mg catalyst with 10 mL of 1 M of HCO_3Na at 80 °C and at 40 bar for 24 h.
[b] Conversion values are calculated from the amount of formate produced from the reaction, which is measured by HPLC.
[c] TON values are calculated using Eq. (3) in Table S3.
[d] 94 μmol/g_{cat} (*i.e.*, less amount) of Pd is loaded on same batch of PDMC-800-16 support material.
[e] 15.0 mg (14 μmol) of Pd/C, 10 wt.% (commercially obtained from Sigma-Aldrich) is used.
[f] Note that the surface area of this material is also high (745 m^2/g) or comparable to those of most of the Pd/PDMC materials.

gas chromatography (GC) (Table S2 and Fig. S4). The result reveals that the dehydrogenation of formate over Pd/PDMC-*T*-*x* catalysts goes through the desirable reaction of $HCO_2^- + H_2O \rightarrow H_2 + HCO_3^-$, without forming the undesired byproduct CO, which sometimes forms from reactions involving formate over some catalysts. In addition, the Pd/PDMC-*T*-*x* catalysts are proven to be easily recyclable and reusable several times without significantly losing their catalytic activity. For example, Pd/PDMC-800-16 is recycled and reused up to at least three times, giving TOF values of 1854 h^{-1}, 1753 h^{-1} and 1477 h^{-1} for the 1st, 2nd and 3rd runs, respectively (Fig. S5a). Consistent with this result, the size of the Pd nanoparticles in the Pd/PDMC-*T*-*x* remain nearly unchanged after recycling (see, for example, the STEM image of Pd/PDMC-800-16 after the 3rd reaction cycle, Fig, S5b). Moreover, tests by ICP-OES for possible leached Pd species in the reaction mixture reveal only < 2 ppm of Pd, indicating the high stability of the Pd/PDMCs catalysts during catalysis.

3.5. *Catalytic properties of Pd/PDMC*-T-x *for* HCO_3^- *hydrogenation*

To assess the ability of Pd/PDMC-*T*-16 materials to promote the H_2 recharging reaction, the hydrogenation of HCO_3^- (to HCO_2^-) in the presence of the materials is evaluated (Table 3) . The catalytic activity of the materials toward this reaction as a function of the pyrolysis temperature used to make them also followed a volcano type trend, in the same way as the result obtained for the dehydrogenation reaction above. Moreover, the Pd/PDMC material synthesized at 800 °C (Pd/PDMC-800-16), once again, shows the best catalytic activity for this reaction, while those prepared either at lower or higher temperatures than 800 °C give lower catalytic activities. The general trend of the materials' catalytic activites for the HCO_3^- hydrogenation reaction are found to be Pd/PDMC-800–16 > Pd/PDMC-700–16 > Pd/PDMC-900–16 > Pd/PDMC-1000–16 » Pd/PDMC-500-16. Notably, the turnover numbers (TONs) of all the Pd/PDMC materials, even the poorly performing ones, are comparable to those of other previously reported Pd-based catalysts for the HCO_3^- hydrogenation reaction (Table S3) [17–21].

An additional control experiment involving a commercially available Pd/C (10 wt.%), whose carbon material does not have N-dopants, was performed (Fig. S6). Despite its high surface area (745 m^2/g) or comparable surface area as those of Pd/PDMC materials, the Pd/C (10 wt.%) shows a significantly lower catalytic activity and gives a lower TOF value than most of the Pd/PDMC materials we have investigated for the hydrogenation reaction (entry 7 in Table 3), just like in the hydrogenation reaction above.

3.6. *Investigation of chemical states of N-dopant sites and their effect on the materials' catalytic properties*

Although Pd nanoparticles are the major species responsible for Pd/PDMCs' catalytic activity toward both reactions, the presence of N-dopant-related species on their carbon support materials must have contributed to their superior catalytic performances. This conclusion is made based on the catalytic results obtained for Pd/PDMC materials and the corresponding control material Pd/C (10 wt.%), which we discussed before.

To further elucidate the effect of N-dopant sites in the Pd/PDMC materials on the materials' catalytic activity, the density and chemical states of nitrogen in the catalysts are analyzed using X-ray photoelectron spectroscopy (XPS) and Raman spectroscopy. The XPS survey spectra show that the atomic ratios of N to C in the Pd/PDMC-*T*-16 catalysts decreases from 11 to 3% when their pyrolysis temperature is raised from 500 to 1000 °C (Fig. 3a). The N1s peak in the spectra can be deconvoluted into four distinct peaks, corresponding to pyridinic-N (398.7 eV), pyrrolic-N (400.3 eV), quaternary-N (401.2 eV), and pyridinic-N^+-O^- (403.3 eV) species [31]. The relative density of the different N-doped species in the materials varies as a function of pyrolysis temperature (Fig. 3b and Fig. S6). The best catalyst for both reactions, Pd/PDMC-800-16, has a relatively higher density of electron-rich pyrrolic-N and pyridinic-N groups than the other Pd/PDMC-*T*-16 materials. Moreover, the density of these groups is higher than the quaternary-N (electron-deficient) species not only in Pd/PDMC-800-16 but all also in all the other Pd/PDMC-*T*-16 materials. On the other hand, the poorly performing catalyst, Pd/PDMC-500-16, has the least density of electron-rich pyrrolic-N and pyridinic-N groups. Since the electron-rich pyrrolic-N and pyridinic-N groups are generally unlikely to form at pyrolysis temperatures less than 600 °C [28–32], their absence in Pd/PDMC-500-16, and thus the material's low catalytic activity, are perhaps not surprising.

The deconvoluted XPS C1s peaks of the Pd/PDMC materials (Fig. S7) also indirectly indicate the presence of O and N species [32]. In the case of the XPS spectra of Pd3d, doublet XPS peaks corresponding to Pd(II) at *ca.* 343.0 eV (Pd $3d_{3/2}$) and 337.6 eV (Pd $3d_{5/2}$) and doublet XPS peaks corresponding to Pd(0) at 340.9 eV (Pd $3d_{3/2}$) and 335.6 eV (Pd $3d_{5/2}$) are observed for all the materials [33,34]. The observed Pd(II) species are most likely due to the presence of Pd-O and/or Pd-N bonds in the materials (Fig. S8). This is further corroborated by extended X-ray absorption fine structure (EXAFS) and near extended X-ray absorption fine structure (NEXAFS) analyses (*vide infra*).

Additionally, the PDMC-*T*-16 materials are characterized by Raman spectroscopy. Their Raman spectra show two first-order bands at 1345 cm^{-1} and 1580 cm^{-1} (Fig. 3c). These correspond to the characteristic D band (which is generally associated with defects in carbon materials, defects that typically stem from the presence of N dopants in such materials) and G band (due to the typical E_{2g} modes) of graphitic carbon materials. The ratio of intensity of the two peaks (I_D/I_G ratio) decreases from 0.97 to 0.91 as the pyrolysis temperature is raised from 500 to 1000 °C, indicating the increase in the degree of graphitization in the PDMC materials at higher pyrolysis temperatures (Fig. 3c and Fig. S9). According to these results, particularly the ones displayed in Fig. 3b and Fig. S6, the different N-dopant-associated species, which are present in the PDMC-*T*-*x* materials, are compiled and illustrated in Fig. 3d.

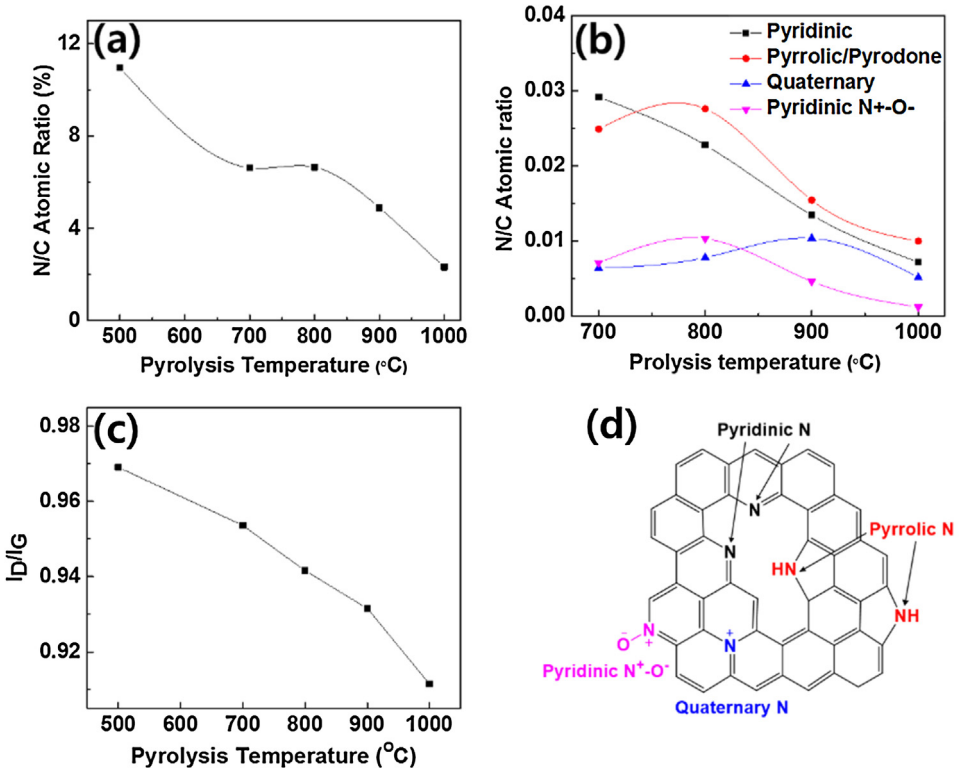

Fig. 3. Results compiled based on XPS and Raman spectra for different Pd/PDMC-*T*-16 materials (where *T* = 500, 700, 800, 900, and 1000 °C): (a) N/C atomic ratio for the total N and C in the materials, (b) N/C ratio for the different types of N species analyzed by XPS, (c) I_D/I_G ratio (ratio of intensity of D and G bands based on Raman spectra), and (d) plausible structures of the N species present in the N-doped carbon materials.

3.7. Investigation of metal–support interactions

To obtain more structural information about Pd/PDMC-*T*-*x* materials, including the possible presence of metal-support interactions in them, the materials are analyzed by EXAFS at Pd K-edge region (Fig. 4 and Table S4) and by NEXAFS (Fig. 5). The coordination numbers (CNs) of Pd–Pd bonding in all the Pd/PDMC-*T*-*x* materials ($CN_{Pd\text{-}Pd} \approx 2$ to 4) are significantly less than that of bulk Pd foil ($CN_{Pd\text{-}Pd} \approx 12$), confirming the presence of well dispersed Pd nanoclusters, each containing only few atoms, on the N-doped carbon support materials. This is also consistent with the observation made by STEM, in which small Pd nanoparticles with an average size of *ca.* 1.6 nm are seen (Fig. 1). In addition, the EXAFS results indicate that the Pd nanoparticles in the PDMC materials are at least partially coordinated with O, N and/or C atoms of the support material, strongly suggesting the presence of metal–support interactions.

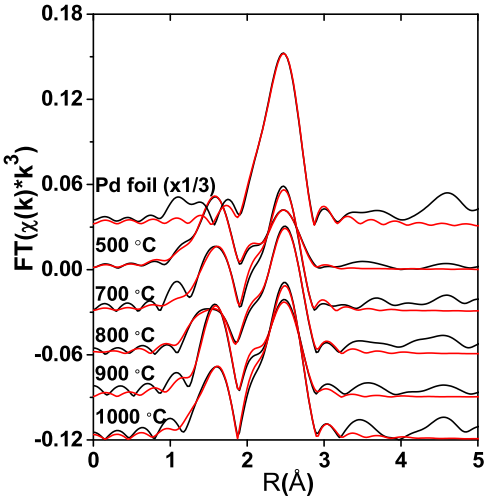

Fig. 4. Fourier transformed EXAFS (black) of Pd/PDMC-*T*-16 materials (where *T* = 500, 700, 800, 900, or 1000 °C) and their best fits (red). (For interpretation of the references to colour in this figure legend, the reader is referred to the web version of this article.).

Among all the Pd-X bond lengths of Pd/PDMC samples, the shortest length, 1.97 Å, is found in Pd/PDMC-800-16 (Table S4). This suggests that the strongest metal–support interaction is present in Pd/PDMC-800-16. The shortest bond length and the strongest metal–support interactions in Pd/PDMC-800-16 (1.97 Å) may have been the result of the relatively higher density of electron rich pyrrolic and pyridinic groups in its N-doped carbon nanostructure.

The interface between Pd nanoparticles and PDMC is further investigated with NEXAFS, and the results are displayed in Fig. 5. In the NEXAFS spectra, Pd/PDMC-800-16 is the only material that shows two different features of peak broadenings, the first at *ca.* 399.4 eV and the second at *ca.* 400.2 eV (Fig. 5b). Both peaks can be assigned to Pd-N type interactions [35], where the unoccupied N2p states hybridize with the Pd4d orbitals [36]. The result suggests that Pd/PDMC-800-16 has a distinct, strong interaction between its Pd nanoparticles and N-species on its support material. This result is in agreement with the one obtained by EXAFS above. So, it is not surprising then that this material is also the one that shows the highest catalytic activity for the HCO_2^-/HCO_3^- reversible reactions.

3.8. Mechanistic studies

To elucidate the plausible reaction pathways by which the reversible HCO_2^-/HCO_3^- reactions take place over Pd/PDMCs, isotopic labeling studies are performed. Specifically three different kinds of isotopic labeling reactions are conducted with Pd/PDMC-800-16. The first one is $D\text{-}CO_2^- + H_2O$, which is named as Reaction

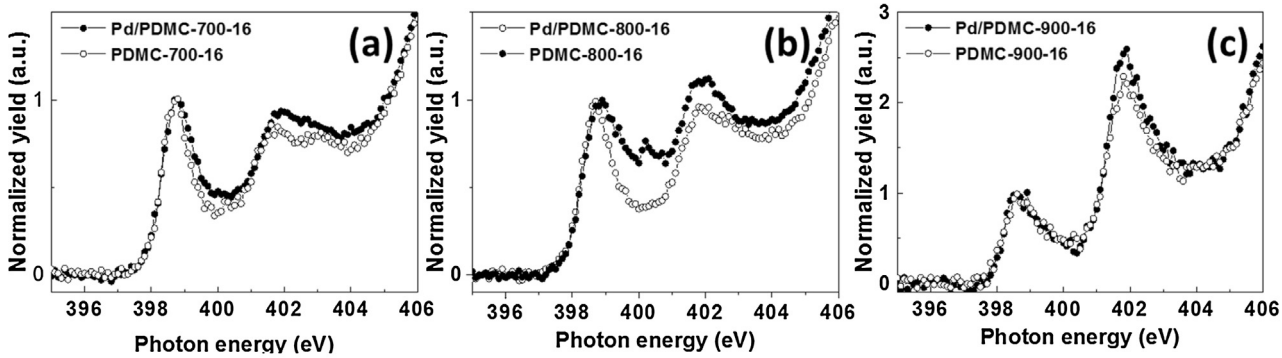

Fig. 5. NEXAFS spectra of (a) Pd/PDMC-700-16, (b) Pd/PDMC-800-16, and (c) Pd/PDMC-900-16, along their corresponding control materials that contain no Pd nanoparticles.

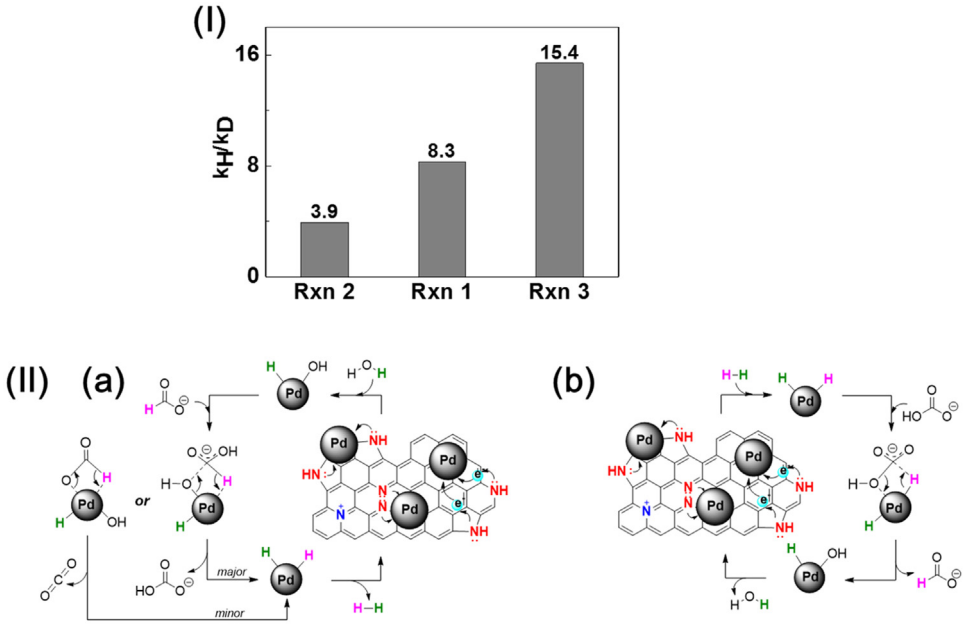

Fig. 6. (I) Results of kinetic isotope effect (KIE) for different reactions over Pd/PDMC-800-16. Rxn 1 is for D-CO_2^- + H_2O, Rxn 2 is for H-CO_2^- + D_2O, and Rxn 3 is for D-CO_2^- + D_2O. (II) Plausible reaction mechanisms for the HCO_2^-/HCO_3^- reversible reactions over the Pd/PDMC materials. The reactions allow reversible H_2 storage/release: a) dehydrogenation pathway and b) hydrogenation pathway. (The pink and green colored H's indicate the H atoms originated from HCO_2^- and H_2O, respectively). The detailed stepwise pathways are further depicted in Scheme S1 in Supporting information section. (For interpretation of the references to colour in this figure legend, the reader is referred to the web version of this article.).

1; the second one is H—CO_2^- + D_2O, which is named as Reaction 2; and the third one is D-CO_2^- + D_2O, which is named as Reaction 3. The reactions are illustrated in detail in Scheme S1. The results from the reactions show kinetic isotope effects (KIEs) (Fig. 6,I), where the values of k_H/k_D follow the trend of: Reaction 3 (15.4) » Reaction 1 (8.3) > Reaction 2 (3.9). The results also indicate that both H_2O and HCO_2^- are involved in the rate-determining step. Moreover, the fact that Reaction 1 gives higher KIE value than Reaction 2 suggests that the bond cleavage of HO—H takes place prior to that of H—CO_2^- during the dehydrogenation reaction (Fig. 6,I). In the reaction mechanism, the final step involves the release of H_2 *via* reductive elimination from the H-Pd-H species [17]. The hydrogenation of HCO_3^- can essentially be thought of as the reverse of the above-discussed HCO_2^- dehydrogenation processes.

Supported by our various experimental methods including XPS, Raman, EXAFS, NEXAFS, and isotopic labeling studies, the reaction mechanisms for the HCO_2^-/HCO_3^- reversible transformations over the Pd/PDMC material are then proposed, as shown in Fig. 6, II. Notably, our results above suggest that the pyridinic/pyrrolic N species formed on the graphitic carbon surfaces upon pyrolysis accelerate the reversible HCO_2^-/HCO_3^- conversions, most likely by donating their electron density to Pd *via* strong metal–support interactions. Moreover, the fact that the Pd nanoparticles in the catalyst are quite small in size, thanks to the synthetic route employed to make them, may have made the materials to show efficient catalytic activity towards the HCO_2^-/HCO_3^- reversible reactions.

4. Conclusion

In summary, we have presented the synthesis of polyaniline (PANI)-derived N-doped mesoporous carbons containing supported Pd nanoparticles (Pd/PDMCs) that show excellent catalytic activity for the HCO_2^-/HCO_3^- reversible reactions. The catalytic activity of the materials has been found to be dependent on their physical properties (*e.g.*, porosity and size of Pd nanoparticles) and chemical compositions (N-dopant associated species) of the materials. The structures and compositions of the catalysts have been controlled and optimized by varying the relative amount of colloidal silica templates and pyrolysis temperatures used to synthesize the materials. In addition, the pyrolysis temperature has been found to cause variations in the local N—C structures of the N-doped carbon support material. The N-dopant-associated species

present in the materials have induced strong metal–support interactions, making the materials to exhibit excellent catalytic activity toward the HCO_2^-/HCO_3^- reversible reactions. The structural and composition parameters identified for the materials in relation to their catalytic properties toward these reversible reactions can provide valuable guidelines for the development of efficient catalysts for H_2-based energy storage/release catalytic systems for H_2-powered fuel cells and related applications.

Acknowledgements

T.A. thanks the US National Science Foundation (NSF) for the financial assistance of this work through DMR-1508611. C.W.Y. acknowledges the financial support from the Technology Development Program to Solve Climate Changes of the National Research Foundation (NRF) funded by the Ministry of Science, ICT & Future Planning (2015M1A2A2074688). P.Z. thanks the financial support from Natural Sciences and Engineering Research Council (NSERC) of Canada. Experiments conducted at Pohang Light Source-II (PLS-II) were supported in part by MEST and POSTECH.

Appendix A. Supplementary data

Supplementary data associated with this article can be found, in the online version, at http://dx.doi.org/10.1016/j.apcatb.2016.10.080.

References

[1] J.A. Turner, Science 305 (2004) 972.
[2] G.W. Crabtree, M.S. Dresselhaus, M.V. Buchanan, Phys. Today 57 (2004) 39.
[3] C. Liu, F. Li, L.-P. Ma, H.-M. Cheng, Adv. Mater. 22 (2010) E28.
[4] N. Armaroli, V. Balzani, Angew. Chem. Int. Ed. 46 (2007) 52.
[5] M. Dadfarnia, P. Novak, D.C. Ahn, J.B. Liu, P. Sofronis, D.D. Johnson, I.M. Robertson, Adv. Mater. 22 (2010) 1128.
[6] J. Graetz, Chem. Soc. Rev. 38 (2009) 73.
[7] L. Li, X. Mu, W. Liu, Z. Mi, C.-J. Li, J. Am. Chem. Soc. 137 (2015) 7576.
[8] M. Yadav, Q. Xu, Energy Environ. Sci. 5 (2012) 9698.
[9] U.B. Demirci, P. Miele, Energy Environ. Sci. 2 (2009) 627.
[10] Ç. Çakanyildirim, M. Gürü, Int. J. Hydrogen Energy 33 (2008) 4634.
[11] F.H. Stephens, V. Pons, R.T. Baker, Dalton Trans. 25 (2007) 2613.
[12] M. Grasemann, G. Laurenczy, Energy Environ. Sci. 5 (2012) 8171.
[13] B. Loges, A. Boddien, F. Gärtner, H. Junge, M. Beller, Top. Catal. 53 (2010) 902.
[14] C. Federsel, R. Jackstell, A. Boddien, G. Laurenczy, M. Beller, ChemSusChem 3 (2010) 1048.
[15] A. Boddien, F. Gärtner, C. Federsel, P. Sponholz, D. Mellmann, R. Jackstell, H. Junge, M. Beller, Angew. Chem. Int. Ed. 50 (2011) 6411.
[16] G. Papp, J. Csorba, G. Laurenczy, F. Joó, Angew. Chem. Int. Ed. 123 (2011) 10617.
[17] H. Wiener, Y. Sasson, J. Blum, J. Mol. Catal. 35 (1986) 277.
[18] B. Zaidman, H. Wiener, Y. Sasson, Int. J. Hydrogen Energy 11 (1986) 341.
[19] Q.-Y. Bi, J.-D. Lin, Y.-M. Liu, X.-L. Du, J.-Q. Wang, H.-Y. He, Y. Cao, Angew. Chem. Int. Ed. 126 (2014) 13801.
[20] J. Su, L. Yang, M. Lu, H. Lin, ChemSusChem 8 (2015) 813.
[21] F. Wang, J. Xu, X. Shao, X. Su, Y. Huang, T. Zhang, ChemSusChem 9 (2016) 246.
[22] J.H. Lee, J. Ryu, J.Y. Kim, S.-W. Nam, J.H. Han, T.-H. Lim, S. Gautam, K.H. Chae, C.W. Yoon, J. Mater. Chem. A 2 (2014) 9490.
[23] K. Koh, J.-E. Seo, J.H. Lee, A. Goswami, C.W. Yoon, T. Asefa, J. Mater. Chem. A 2 (2014) 20444.
[24] J. Zhang, Z. Zhao, Z. Xia, L. Dai, Nat. Nanotechnol. 3 (2013) 1114.
[25] J.S. Yoo, Z.-J. Zhao, J.K. Nørskov, F. Studt, ACS Catal. 5 (2015) 6579.
[26] G. Wu, A. Santandreu, W. Kellogg, S. Gupta, O. Ogoke, H. Zhang, H. Wang, L. Dai, Nano Energy (2015), http://dx.doi.org/10.1016/j.nanoen.2015.12.032.
[27] Y. Liu, Z. Jin, J. Wang, R. Cui, H. Sun, F. Peng, L. Wei, Z. Wang, X. Liang, L. Peng, Y. Li, Adv. Funct. Mater. 21 (2011) 986.
[28] R. Silva, D. Voiry, M. Chhowalla, T. Asefa, J. Am. Chem. Soc. 135 (2013) 7823.
[29] H.-W. Liang, W. Wei, Z.-S. Wu, X. Feng, K. Müllen, J. Am. Chem. Soc. 135 (2013) 16002.
[30] J. Yue, A.J. Epstein, Z. Zhong, P.K. Gallagher, A.G. Macdiarmid, Synth. Met. 41 (1991) 765.
[31] J.R. Pels, F. Kapteijn, J.A. Moulijin, Q. Zhu, K.M. Thomas, Carbon 33 (1995) 1641.
[32] P.H. Matter, L. Zhang, U.S. Ozkan, J. Catal. 239 (2006) 83.
[33] G. Kumar, J.R. Blackburn, R.G. Albridge, W.E. Modde-man, M.M. Jones, Inorg. Chem. 11 (1972) 296.
[34] V.B. Parambhath, R. Nagar, S. Ramaprabhu, Langmuir 28 (2012) 7826.
[35] S. Kaneko, M. Kiguchi, In Fullerenes, Nanotubes and Carbon Nanostructures, vol. 22, Taylor & Francis Group, LLC., 2014, pp. 765.
[36] F. Pinakidoua, M. Katsikinia, E.C. Palouraa, A. Akbarib, J.P. Rivviereb, Mater. Sci. Eng. B 176 (2011) 473.